ACADEMIC PRESS

Available online at www.sciencedirect.com
SCIENCE DIRECT®

Journal of Solid State Chemistry 170 (2003) 221–226

JOURNAL OF SOLID STATE CHEMISTRY

http://elsevier.com/locate/jssc

Preparation and characterization of spherical V_2O_3 nanopowder

Chenmou Zheng,[a,*] Xinmin Zhang,[a] Shan He,[b] Qun Fu,[a] and Deming Lei[b]

[a] *School of Chemistry and Chemical Engineering, Zhongshan University, Guangzhou 510275, People's Republic of China*
[b] *Department of Physics, Zhongshan University, Guangzhou 510275, People's Republic of China*

Received 5 February 2002; received in revised form 27 August 2002; accepted 12 September 2002

Abstract

V_2O_3 nanopowder with spherical particles was prepared by reducing pyrolysis of the precursor, $(NH_4)_5[(VO)_6(CO_3)_4(OH)_9]\cdot 10H_2O$, in H_2 atmosphere. The thermolysis process of the precursor in a H_2 flow was investigated by thermogravimetric analysis and differential thermal analysis. The results indicate that pure V_2O_3 forms at 620°C and crystallizes at 730°C. The effects of various reductive pyrolysis conditions on compositions of V_2O_3 products were studied. Scanning electron micrographs show that the particles of the V_2O_3 powder obtained at 650°C for 1 h are spherical about 30 nm in size with more homogeneous distribution. Experiments show that nanopowder has larger adsorption capacity to gases and is more easily reoxidized by air at room temperature than micropowder. Differential scanning calorimetry experiment indicates that the temperature of phase transition of nano-V_2O_3 powder is −119.5°C on cooling or −99.2°C on heating. The transition heats are $-12.55\,J\,g^{-1}$ on cooling and $11.42\,J\,g^{-1}$ on heating, respectively.

Keywords: Ammonium oxovanadium (IV) carbonato hydroxide; Thermoanalysis and pyrolysis in hydrogen; Spherical V_2O_3 nanopowder; Route of precursor

1. Introduction

The V_2O_3 system has been the subject of many investigations because it exhibits one or more sets of spectacular metal–insulator transitions. Pure V_2O_3 shows a first-order phase transition at about −120°C [1]. With addition of a few percent Cr [1], Al [2] or RE [3], a discontinuity in resistivity occurs in the range −100–200°C. These properties allow them to be used in many different devices such as temperature sensors and current regulation [4,5]. V_2O_3 powder is also used in conductive polymer composites [6] and in catalysts [7]. It has become apparent that the powder particle characteristics such as particle size, particle size distribution and morphology as well as powder surface chemistry have great influence on the final properties of the materials and devices; further properties of powder are directly related to its preparation methods.

Over two decades, many methods for preparing various V_2O_3 powders have been studied [8–14], such as preparing spherical V_2O_3 particles by O_2–H_2 flame fusion of V_2O_3 at 2000°C [8], synthesizing spherical and necking V_2O_3 powder by reducing V_2O_5 obtained by evaporative decomposition of solutions in H_2 atmosphere at 850°C for 6 h [9], pyrolyzing the hydrazine-containing vanadium salt [10], and reducing the sol–gel-synthesized V_2O_5 in H_2 stream [11]. However, only micropowder could be obtained by these methods.

So far, only one report has been found in the literature on the synthesis of V_2O_3 nanoparticles by laser-induced vapor-phase reaction [15]. In this work, we report a novel method for preparing nano-V_2O_3 powder with spherical particles and more homogeneous distribution by reductive pyrolysis of ammonium oxovanadium(IV) carbonato hydroxide, $(NH_4)_5[(VO)_6(CO_3)_4(OH)_9]\cdot 10H_2O$, in a H_2 flow. The choice of this compound as the precursor is based on the following considerations: (1) the precursor is easily synthesized, (2) V_2O_3 nanoparticles are expected to be obtained easily due to the release of large amount of gases during pyrolysis of the precursor, (3) pyrolysis temperature reduction will be lower, and (4) the as-prepared V_2O_3 will not contain any impurity because the non-vanadium

*Corresponding author. Fax: +020-8411-2245.
E-mail address: cedc46@zsu.edu.cn (C. Zheng).

0022-4596/03/$ - see front matter © 2002 Elsevier Science (USA). All rights reserved.
PII: S0022-4596(02)00038-5

components, nitrogen and carbon, in the precursor possess volatility during pyrolysis.

2. Experimental section

2.1. Synthesis of the precursor

The synthesis route of the precursor was reported in an earlier work of ours [16]

$$V_2O_5 + HCl + N_2H_4 \cdot 2HCl \rightarrow VOCl_2 + NH_4HCO_3 \rightarrow (NH_4)_5[(VO)_6(CO_3)_4(OH)_9] \cdot 10H_2O.$$

The purities of the starting material V_2O_5 (CP) and the precursor were determined by inductively coupled plasma-atomic emission spectroscopy. The impurity content of V_2O_5 is atomically about 1000 ppm, with Cr, Sb, and Ga as the main sources of impurities. The total impurity content of the precursor amounted to atomically about 100 ppm (calculated as total impurity/vanadium). This shows that the materials used in this study were purified in the synthesis process of the precursor.

2.2. Thermoanalysis of the precursor

The sample of the precursor used here was about 10 μm in size. Its composition was confirmed with its molecular formula. Thermogravimetric analysis (TGA) and differential thermal analysis (DTA) were simultaneously conducted on a PCT-1-type combined thermoanalysis meter, with 5°C min^{-1} heating rate and in a H_2 (99.999%) flow of 15 mL min^{-1}.

2.3. Reduction pyrolysis of the precursor

A coarse precursor was pulverized to $\leqslant 2$ μm in size. Its vanadium content was higher than the calculated value by about 2.6%. The fine precursor was spread in a 130-mm long, 18-mm diameter quartz boat. The quartz boat was placed in a Φ23-mm silica tube. A stream of N_2 (99.999%) was introduced into the system to replace the air in the tube, then a stream of H_2 (99.999%) replaced the N_2 flow. The tube was heated to a desired temperature (350–900°C) and maintained for a preset time. The heating rate was 26°C min^{-1}. After the reaction was completed, the silica tube was pulled out of the tube furnace and cooled rapidly in air to room temperature in a H_2 stream. The V_2O_3 samples were placed in an evacuated desiccator with P_2O_5 to prevent them from being reoxidized and adsorbing moisture.

2.4. Characterization of the products

The elementary analysis of V_2O_3 was carried out on a Perkin-Elmer VARIO-EL. Nitrogen was also determined using the Kjeldahl technique [17]. The results show that no of N and C were detected. V_2O_3 samples were dissolved in a mixed solution of phosphoric–sulfuric acid under CO_2 atmosphere for determining the V^{3+} and total vanadium content. The content of V^{3+} was determined by a $K_2Cr_2O_7$ solution volumetrically using ferroin as an indicator [18]. The total vanadium content was titrated by a $FeSO_4$ solution volumetrically. In comparison with the usual method of oxidizing V_2O_3 to V_2O_5 by thermogravimetric method, the result in ratio of V^{3+}/V_{total} by this method is estimated to be lower by 0.5%. The adopted ratio of V^{3+}/V_{total} in this paper was already corrected by thermogravimetric method. Desorption of powder to gases was conducted on NETZSCH TG 209 TGA meter in an Ar (99.99%) flow of 20 mL min^{-1}, with a heating rate of 10°C min^{-1}. X-ray diffraction (XRD) experiments were carried out on a D/max-3A diffractometer using Cu$K\alpha$1 radiation ($\lambda = 0.154050$ nm). The morphologies of the products were observed on a JSM-6330F field emission scanning electron microscope (SEM). Differential scanning calorimetry (DSC) experiments were performed on a NETZSCH DSC-204 in N_2 atmosphere in the range −170–20°C with a heating or cooling rate of 10°C min^{-1}.

3. Results and discussion

3.1. Thermoanalysis of the precursor

The TGA and the DTA curves of the precursor are shown in Fig. 1. The thermolysis models from the TGA curve are displayed in Scheme 1. The TGA data from Fig. 1 and Scheme 1 indicate that there are five intermediates A, B, C, D, and E before V_2O_3 (F) forms at 620°C in the reductive pyrolysis process of the precursor. It can be seen from Fig. 1 that there are eight endothermic peaks on the DTA curve due to the thermolysis effects of the formation of the intermediates. The sharp peak at 70°C is due to the formation of A. The peak at 115°C is due to the formation of B. The two peaks at 135°C and 167°C are due to the formation of C. The broad peak at 340°C is due to the formation of D ($VO_2 \cdot H_2O$). And the three small peaks at 420°C, 412°C, and 440°C are due to the formation of E ($VO_2 \cdot 0.5H_2O$). However, the endothermic peak corresponding to the dehydration effect of $VO_2 \cdot 0.5H_2O$ formed at 465°C shown in the Scheme 1 is not observed on the DTA curve. The large exothermic peak at 612°C on the DTA curve is attributed to the exothermic effect of reduction of V^{4+} to V^{3+}. This is consistent with the result of the TGA. According to the data in Scheme 1, the experimental value of residual weight percentage (56.2%) of $VO_2 \cdot H_2O$ is lower than its calculated value (56.9%). This implies that V^{4+} has been lightly reduced at <390°C. This deduction is confirmed by a pyrolysis

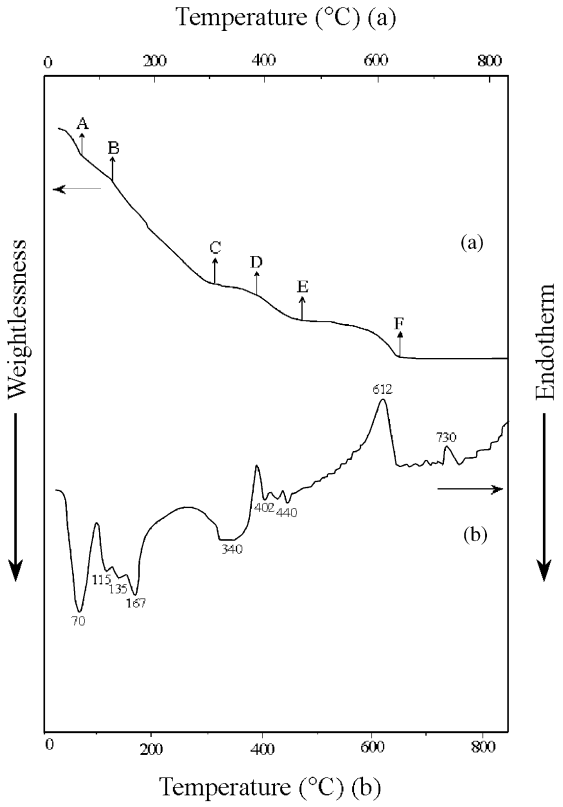

Fig. 1. TGA and DTA curves of thermoanalysis of the precursor run at 5°C min^{-1} in H_2 flow: (a) TGA curve and (b) DTA curve.

of the precursor at 350°C for 30 min under H_2 in a silicon tube, in which the ratio of V^{3+}/V_{total} of the product is 0.06 (see curve (a) in Fig. 2). Since the exothermic effect of forming V_2O_3 was large, the endothermic peak of dehydration of $VO_2 \cdot 0.5H_2O$, which may occur in the range 470–620°C according to the TGA curve, is submerged in the exothermic peak of 612°C. The small exothermic peak at 730°C on the DTA curve is attributed to the crystallization of V_2O_3.

Reduction of bulk particle V_2O_5 was studied by thermal analysis in pure H_2 stream and showed that pure V_2O_3 formed at 717°C [19]. Obviously, this temperature is higher than that of forming V_2O_3 in the thermolysis of the precursor by 97°C, showing that the nanoparticles in the thermolysis process of the precursor have higher reduction activity than that of the V_2O_5 bulk particles. Most importantly, the difference between the formation and the crystallization temperatures (620°C and 730°C) of V_2O_3 is large enough to be detected in the thermolysis process of the precursor. This is the first report for the crystallization temperature of V_2O_3.

3.2. Reduction pyrolysis of the precursor

The effect of various reductive pyrolysis conditions on composition of V_2O_3 product is shown in Figs. 2 and 3.

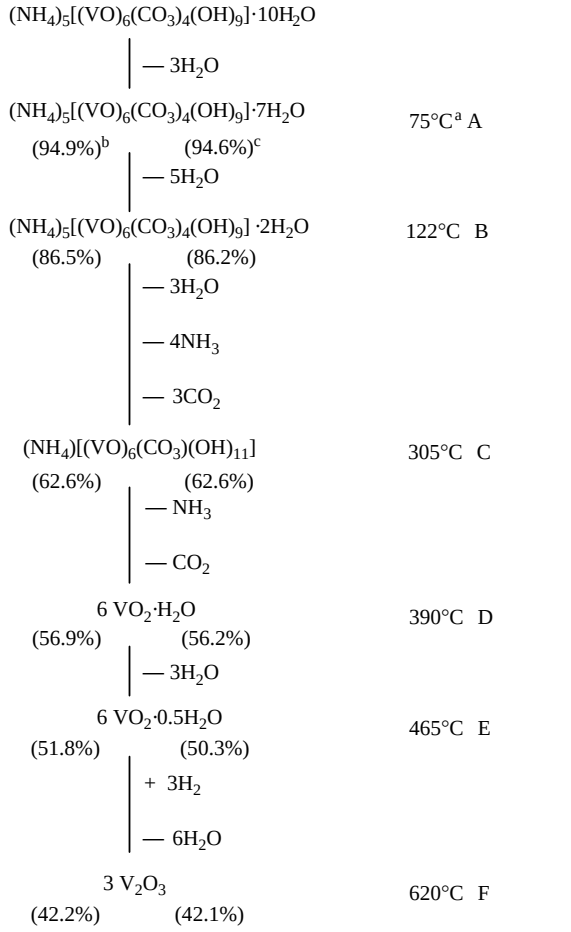

Scheme 1. Thermolysis process of the precursor: (a) the temperature of formation of intermediate; (b, c) the calculated and the experimental value of residual weight percentage, respectively.

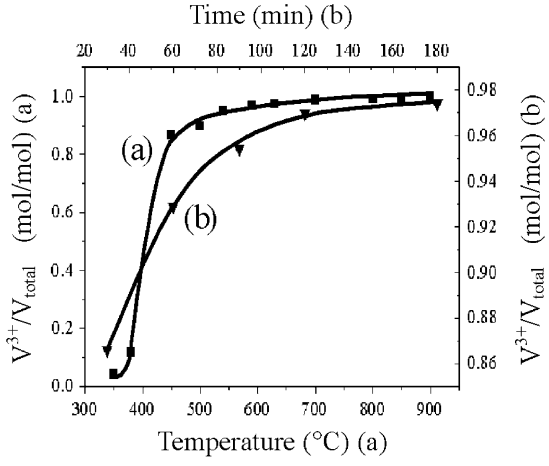

Fig. 2. Effects of pyrolysis temperature and time on product composition: (a) precursor 1.5 g, H_2 0.118 cm s^{-1}, pyrolysis for 30 min and (b) precursor 1.5 g, H_2 0.118 cm s^{-1}, pyrolysis at 450°C.

Fig. 2 indicates that under the same pyrolysis conditions the ratio of V^{3+}/V_{total} of product is increased with increasing temperature or prolonged reaction time.

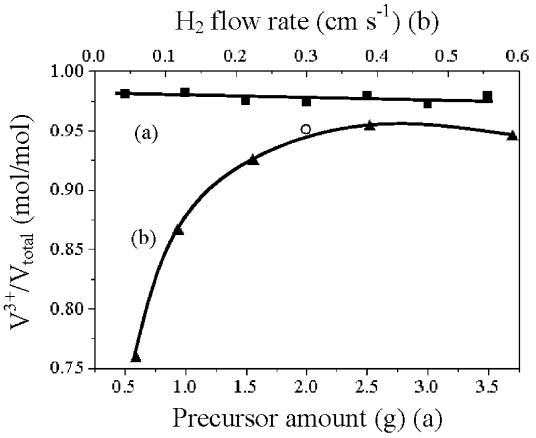

Fig. 3. Effect of precursor amount and H_2 flow rate on product composition: (a) H_2 0.118 cm s^{-1}, 650°C for 30 min and (b) precursor 1.5 g, 450°C for 30 min.

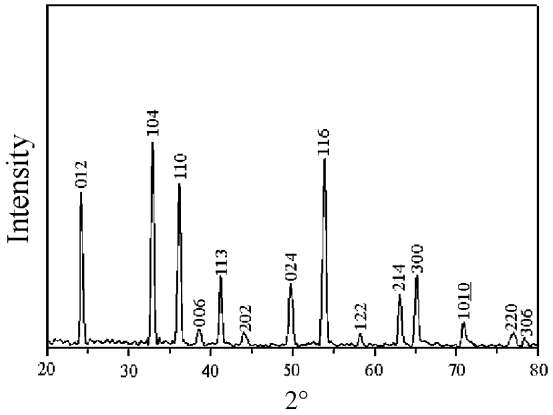

Fig. 4. XRD pattern of V_2O_3 obtained at 650°C for 1 h.

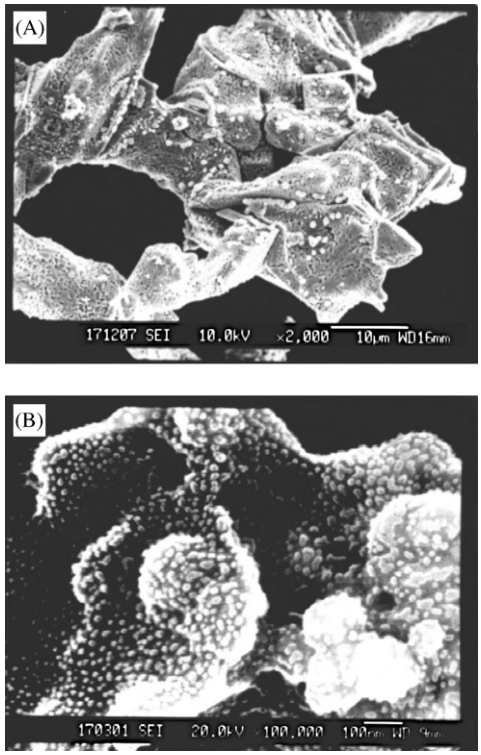

Fig. 5. SEM micrographs of V_2O_3 powders: (a) obtained by reducing V_2O_5 at 900°C for 5 h and (b) obtained by pyrolysis of the precursor at 650°C for 1 h.

However, the increasing of the ratio is very slow as it reaches 0.95. One can see from curve (a) in Fig. 2 that the ratio of 0.948 at 540°C for 30 min only increased to the ratio of 0.998 at 900°C for 30 min. The curve (a) in Fig. 3 shows that the ratio of V^{3+}/V_{total} is not obviously influenced by precursor amount. For the curve (a) in Fig. 3, the point expressed in circle is the result of 1.1 g V_2O_5 instead of 2.0 g precursor. It shows again that the nanoparticles are far easier to be reduced than the microparticles, especially in the case of V^{3+}/V_{total} ratio over 0.95. The curve (b) in Fig. 3 shows that the ratio of V^{3+}/V_{total} is increased as the H_2 flow rate increases, but is lightly decreased as the H_2 flow rate is over 0.389 cm s^{-1}. The late effect may be caused by the weak adsorption of particles to H_2. Therefore, it is necessary to control the flow rate of H_2.

3.3. Properties and morphology of V_2O_3 powder

The XRD pattern of the V_2O_3 powder obtained at 650°C for 1 h is shown in Fig. 4, in which no peaks of impurities are observed.

Fig. 5a is a SEM micrograph of V_2O_3 micropowder obtained at 900°C by reducing V_2O_5 powder. Its particle size is about 14×20 μm^2. It can be seen that the microparticles have many holes with 50–250 nm in size and some spherical nanoparticles about 100–500 nm adhering to their surfaces. Fig. 5b is a SEM micrograph of V_2O_3 powder obtained by the pyrolysis of the precursor at 650°C for 1 h, in which the sample was prepared by dispersing the powder in a 731DP super-dispersing agent solution. One can see from the picture that the spherical particles with about 30 nm size are clear and more homogeneous in distribution even if there is still trace of dispersing agent. The particle size evaluated from the picture is consistent with the mean value 33.2 nm calculated by the Scherrer equation. V_2O_3 nanopowder is expected to be easily prepared by the pyrolysis of the precursor, because a large amount of gases is releasing and the reduction occurs during the pyrolysis. This process causes strong splitting and atomization of the particles. Moreover, the gases adsorbed on the particle surface also inhibit the particles from sintering and further growing. However, the formation of the spherical particles is unexpected. This may be related to the crystallization habits and the characteristics of the nanoparticles. It can be seen from Fig. 5a that the nanoparticles on the surface of microparticles spheroidize.

The thermogravimetric experiments of nano- and micropowders in a 99.99% Ar stream in Fig. 6 indicate their desorption to gases and reoxidation effect. The results are listed in Table 1. There is a plateau on curve (a) and (b) around 180°C and 230°C in Fig. 6, respectively, the corresponding weightlessness mass is 0.34% and 0.14%. This weightlessness mass is defined as the adsorptive capacity to gases of powder and corresponding temperature is defined as temperature of ending desorption. The results in Table 1 indicate that the adsorptive capacity of the nanopowder is 2.4 times as large as that of the micropowder. At the same time, the mass of the former increases rapidly as the temperature is higher than 185°C and the mass of the latter increases slowly until the temperature is higher than 245°C, indicating that the nanopowder is more easily reoxidized by trace of oxygen in the Ar flow. Due to the peculiar particle structure of the micropowder with many nanoholes, the temperature (230°C) of ending desorption for the micropowder is higher than that (180°C) for the nanopowder. To observe the reoxidation effect of various powders further, three kinds of powder were exposed to air and then their changes in composition were determined. As Fig. 7 shows, the reoxidation rate of the micropowder of $14 \times 20\,\mu m^2$ size (curve (a)) is lightly slower than that of the nanopowder of <100 nm size (curve (b)), and the reoxidation rate of another nanopowder of about 36 nm size (curve (c)) is very fast.

Botto et al. [20–22] indicated that it was very difficult to obtain pure V_2O_3 even with freshly prepared samples in their studies on V_2O_3 by IR, XPS and EPR, because of the reoxidation by the effect of air at the surface of the particles. Obviously, nanopowders, especially obtained at lower temperature, more easily adsorb air because of their finer size, larger surface area and stronger adsorption property, causing deeper reoxidation when exposed to air. This is why the formation of pure V_2O_3 is observed in the thermoanalysis process and pure V_2O_3 powder cannot be obtained under stronger conditions in the pyrolysis process. For example, the ratio of V^{3+}/V_{total} of the fresh sample obtained at 900°C for 5 h is only 0.993 for a bulk sample in Fig. 7. Even using V_2O_5 as the original material, the ratio of V^{3+}/V_{total} of the fresh sample obtained at the same conditions still is 0.999.

DSC of V_2O_3 powder has not been determined up to now. The DSC curves of V_2O_3 nanopowder in Fig. 8 show that the temperatures of phase transition are −119.5°C on cooling and −99.2°C on heating, respectively. These are consistent with the results observed by determination of electrical resistance (1). According to the DSC, the transition heat is $-12.55\,J\,g^{-1}$ on cooling or $11.42\,J\,g^{-1}$on heating, respectively, in this work.

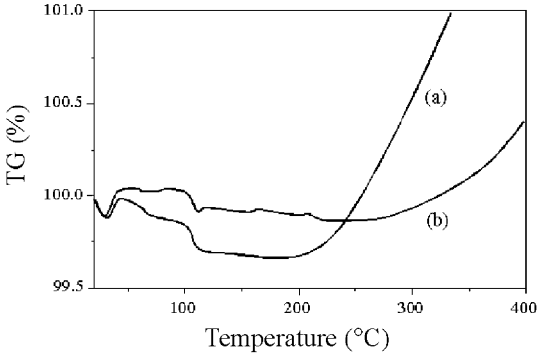

Fig. 6. Thermogravimetric curves of V_2O_3 powders in an Ar flow: (a) obtained by pyrolysis of the precursor at 650°C for 30 min and (b) obtained by reducing V_2O_5 at 900°C for 5 h.

Table 1
The data of thermogravimetric curves of V_2O_3 powders shown in Fig. 6

Sample	Adsorption capacity (%)	Temperature of ending desorption (°C)	Reoxidation temperature (°C)
Nanopowder	0.34	180	185
Micropowder	0.14	230	245

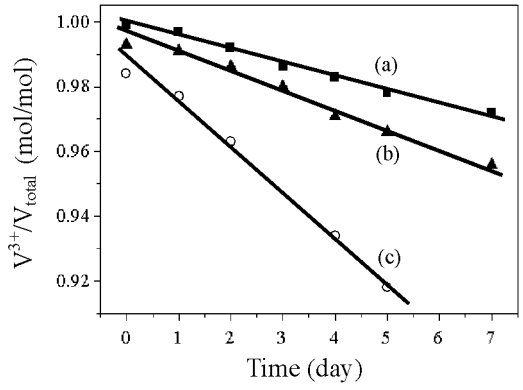

Fig. 7. Reoxidation process of V_2O_3 powders in air: (a) micropowder from reducing V_2O_5 at 900°C for 5 h, (b) nanopowder from pyrolysis of the precursor at 900°C for 5 h, and (c) nanopowder from pyrolysis of the precursor at 700°C for 1 h.

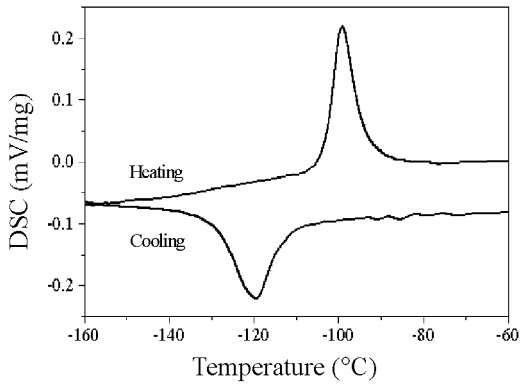

Fig. 8. DSC scans of V_2O_3 nanopowder.

4. Conclusion

The thermoanalysis and pyrolysis of polycrystalline $(NH_4)_5[(VO)_6(CO_3)_4(OH)_9]\cdot 10H_2O$ under H_2 atmosphere show that it is a very good precursor with the advantages of easy preparation, purification and production, yielding spherical nanometer-sized V_2O_3 powder under mild conditions. The formation and crystallization temperatures of pure V_2O_3 at 620°C and 730°C, respectively, are first observed. In comparison with reduction of V_2O_5 to V_2O_3 by H_2, the precursor is far easier to be reduced completely at a lower temperature and in a shorter time, due to the high activity of the formation of nanoparticles during reductive pyrolysis of the precursor. Nano-V_2O_3 powder is more easily reoxidized by air in room temperature than micro-V_2O_3 powder, but the effect can be effectively decreased by raising temperature or prolonging the time of pyrolysis of the precursor. Temperature and heat of phase transition of nano-V_2O_3 powder were first determined by DSC. The temperatures of transition on cooling and heating are consistent with the results obtained by determination of electrical resistance reported in the literature.

Acknowledgment

This work was supported by the Natural Science Foundation of China (NO. 59972045).

References

[1] R.H. Kokbi, M. Rapeaur, A.J. Aymami, G. Desgardin, Mater. Sci. Eng. B 38 (1996) 80.
[2] M.G. Joshi, M.J. Honig, Rev. Chim. Mineral. 19 (1982) 251.
[3] T. Suzuki, M. Ogino, T. Yoshizuka, K. Kunihara, K. Tsuda, Adv. Sci. Technol. (Faenza, Italy) 17 (1999) 135.
[4] E. Andrich, Electron. Appl. 26 (1996) 123.
[5] S.R. Perkins, A. Rüegg, M. Fischer, Adv. Ceram. 7 (1983) 166.
[6] Y. Pan, G. Wu, X. Yi, J. Mater. Sci. 29 (1994) 5757.
[7] L.G. Vader, J. Catal. 98 (1986) 522.
[8] S. Kittaka, S. Sasaki, T. Morimoto, J. Mater. Sci. 22 (1987) 557.
[9] J.R. Sullivan, T.T. Srinivasan, E.R. Newnham, J. Am. Ceram. Soc. 73 (1990) 3715.
[10] J. Wu, H. Liu, S. Zhu, Z. Ma, China Chem. Lett. 2 (1991) 901.
[11] J. Piao, S. Takahashi, S. Kohiki, Jpn. J. Appl. Phys. Part. 1 37 (1998) 6519.
[12] Y. Ueda, K. Kosuge, S. Kachi, J. Solid State Chem. 31 (1980) 171.
[13] G. Li, J. Li, J. Chengdu Keji Univ. 3 (1984) 27.
[14] A. Mukheriee, J. Less-Common Met. 107 (1985) 89.
[15] O. Toshiyuki, I. Yasuhiro, K.R. Kenkyu, J. Photopolym. Sci. Technol. 10 (1997) 211.
[16] W.C.T. Mak, P. Li, C. Zheng, K. Huang, J. Chem. Soc., Chem. Commun. 1597 (1986).
[17] I.A. Vogel, in: I.A. Vogel, Ed., Quantitative Inorganic Analysis, 3rd Edition, Wiley, New York, 1961, p. 312.
[18] G.G. Rao, K.P. Rao, Talanta 13 (1966) 1335.
[19] D. Ballivet-Tkatchenko, G. Delahay, J. Thermal Anal. 41 (1994) 1141.
[20] L.I. Bott, B.M. Vasollo, J.E. Baran, M.G. Minelli, Mater. Chem. Phys. 50 (1997) 267.
[21] J. Mendialdua, R. Casanova, Y. Barbaux, J. Electron Spectrosc. Relat. Phenom. 71 (1995) 249.
[22] T. Hirata, H.Y. Zhu, J. Phys.: Condens. Matter 4 (1992) 7377.